Nanosphere Lithography: Effect of the External Dielectric Medium on the Surface Plasmon Resonance Spectrum of a Periodic Array of Silver Nanoparticles

Traci R. Jensen, Michelle L. Duval, K. Lance Kelly, Anne A. Lazarides, George C. Schatz,*,† and Richard P. Van Duyne*,‡

Department of Chemistry, Northwestern University, Evanston, Illinois 60208-3113

Received: July 29, 1999

In this paper we examine the effect of solvent on the optical extinction spectrum of periodic arrays of surface-confined silver nanoparticles fabricated by nanosphere lithography (NSL). By use of NSL, it is possible to systematically vary the out-of-plane height of the nanoparticles, and by thermal annealing, we can control the nanoparticle shape. We have studied four separate samples of nanoparticle arrays; three samples have nanoparticles that are truncated tetrahedral in shape but that differ in out-of-plane height and one sample has nanoparticles that are oblate ellipsoidal in shape. By performing UV−vis extinction spectroscopy measurements at 12 μm spatial resolution, we show that the defect sites that occur as a byproduct of the NSL fabrication process play a negligible role in the macroscale extinction spectrum. We find that the extinction spectrum of the nanoparticles that are oblate ellipsoidal in shape is least sensitive to the surrounding dielectric medium, and the extinction spectrum of the nanoparticles that are truncated tetrahedral in shape with the smallest out-of-plane height is most sensitive. A 1 nm shift in the extinction maximum corresponds to a 0.005 change in the refractive index of the external medium. Theoretical calculations based on the discrete dipole approximation (DDA) are presented. The DDA is a coupled finite element method capable of calculating the extinction of light for particles of arbitrary shape and size. The discrepancy between the experimental and theoretical results is small for the oblate ellipsoidal-shaped particle but progressively increases for the truncated tetrahedral-shaped particles as they become more oblate. This discrepancy is lessened by including the effect of substrate−particle interactions in the calculation. The DDA theory predicts a significantly larger red shift in the extinction maximum with increasing solvent refractive index than is observed experimentally.

I. Introduction

The optical response of noble metal nanoparticles is often characterized by the presence of a strong absorption band that is absent from the spectrum of the bulk metal. This is attributed to a resonance in the collective motion of the conduction electrons in response to an incident electromagnetic field and is called the localized surface plasmon resonance, hereafter referred to simply as the surface plasmon resonance (SPR). The SPR is dependent on the size, shape, and degree of particle−particle coupling of the nanoparticles, the dielectric properties of the metal from which the nanoparticles are composed, and the dielectric properties of the local environment in which the nanoparticles are immersed.[1] Until recently, it has been difficult to control and characterize the first three of these parameters in order to systematically study their effect on the observed UV−vis extinction spectra of nanoparticles. The SPR plays a key role in determining the magnitude of the enhancement factor in surface-enhanced Raman scattering (SERS) and other surface-enhanced spectroscopies, according to the electromagnetic mechanism.[2] Thus, the ability to understand and control the SPR of nanoparticles will provide unprecedented levels of insight into their surface-enhancing properties.

Surface plasmon resonance spectra have been measured from metal colloids as a function of particle size and average interparticle spacing in solution,[3−6] but in these systems it is difficult if not impossible to systematically vary the particle shape or the solvent in which the particles are immersed. The absorbance of metal clusters deposited onto a substrate in a vacuum has also been studied,[7] and in this case it is possible to vary cluster size and the dielectric constant of the surrounding matrix. However, this method is limited to small nanoparticles, and particle shape and interparticle spacing are difficult to vary systematically over a large range. The UV−vis extinction of metal island films has been studied,[8−11] but it is difficult to quantify the results, since these films contain a broad distribution of particle shapes and sizes. Using a template-controlled electrochemical deposition procedure, Martin et al.[12,13] have examined the optical properties of metal nanoparticles within an alumina host matrix as a function of particle size and aspect ratio. Nanolithographic methods for preparing arrays of particles on a substrate provide an ideal way to systematically study the effects of particle size, shape, spacing, and surrounding dielectric medium. Using electron beam lithography, Aussenegg and co-workers[14,15] have prepared arrays of silver nanoparticles and have studied the effect of aspect ratio and interparticle spacing on the surface plasmon resonance spectra. Ferrell et al.[16] have produced arrays of silver ellipsoidal particles and have measured their optical properties as a function of particle aspect ratio.

Nanosphere lithography (NSL) is an ideal fabrication tool for producing regular, nearly homogeneous arrays of nanoparticles with tunable shapes, sizes, and spacings.[17−19] The method involves drop-coating a suspension of polystyrene nanospheres

* To whom correspondence should be addressed.
† E-mail: schatz@chem.nwu.edu.
‡ E-mail: vanduyne@chem.nwu.edu.

10.1021/jp9926802 CCC: $18.00
Published on Web 10/23/1999

onto a substrate and allowing them to self-assemble into a hexagonal close-packed monolayer. The monolayer of nanospheres acts as a deposition mask through which a metal is deposited. The nanosphere mask is then removed, leaving behind an array of metal nanoparticles. When the size of the polystyrene nanospheres and the amount of material deposited are controlled, independent tuning of the width and height of the nanoparticles is allowed. A postdeposition annealing procedure can be used to change the in-plane shape of the nanoparticles. Although it is not utilized in this work, angle-resolved NSL can be used to control interparticle spacings, sizes, and shapes.[20]

In this paper we have used nanosphere lithography to fabricate particles with varying heights and in-plane shapes with which we can systematically study the effect of the external dielectric constant on the surface plasmon resonance spectra. To the best of our knowledge, the effect of solvent has only been experimentally addressed for metal island films, colloids, and small clusters. We present results from both macroscale and microscale (spatially resolved) UV−vis measurements to support our contention that we are probing the surface plasmon resonances of the nanoparticles themselves and not those of the defect sites that are present in the NSL-fabricated nanoparticle arrays. The SPR spectra are modeled using an implementation of electrodynamic theory known as the discrete dipole approximation (DDA). In a previous paper,[19] we have shown the utility of the DDA in modeling the SPR spectrum of a periodic array of nanoparticles produced via nanosphere lithography.

The remainder of this manuscript is organized as follows. In section II we will discuss the experimental details of fabricating the nanoparticle arrays and of measuring their structural properties and optical extinction spectra. In section III we will present experimental results, and in section IV we will introduce and attempt to apply the DDA theory to understand the experimental results. In section V we will summarize our results and conclusions.

II. Experiment

A. Materials. Ag (99.99%, 0.50 mm diameter) was purchased from D. F. Goldsmith (Evanston, IL). Ruby red muscovite mica was purchased from Asheville-Schoonmaker (Newport News, VA) in the form of 50 μm thick sheets. It was cut either into 1 in. diameter circular disks for use in the liquid cell or into approximately 1 cm^2 squares. Polystyrene nanospheres (400 ± 7 nm diameter) were obtained from Interfacial Dynamics Corporation (Portland, OR). Tungsten vapor deposition boats were purchased from R. D. Mathis (Long Beach, CA). Acetone, methanol, cyclohexane, methylene chloride, carbon tetrachoride, and pyridine were used as received from Aldrich Chemical Co. (Milwaukee, WI). Nitrogen used for drying was purchased from Air Products and passed through a particulate filter and a tube packed with Drierite (W. A. Hammond Drierite Co., Xenia, OH) before use.

B. Preparation of Periodic Particle Arrays. Single-layer periodic particle arrays (PPAs) were prepared by nanosphere lithography as previously described.[17−19] Polystyrene nanospheres were received as a suspension in water and further diluted in a 1:1 ratio with a solution of the surfactant TritonX-100 and methanol (1:400 by volume). An aliquot of this suspension was drop-coated onto the substrate and allowed to dry. The nanospheres self-assembled to form a hexagonal close-packed monolayer that acts as a material deposition mask. Substrates were then mounted into the chamber of a vapor deposition system (Consolidated Vacuum Corporation). Silver was deposited at a rate of 0.2 nm/s, as measured by a Leybold Inficon (East Syracuse, NY) XTM/2 quartz crystal microbalance deposition monitor. After deposition, the samples were sonicated for 2 min in methylene chloride to remove the polystyrene nanosphere mask, leaving behind a hexagonal array of silver nanoparticles. Postdeposition annealing was performed on some samples by heating at 300 °C for 1 h in a vacuum.

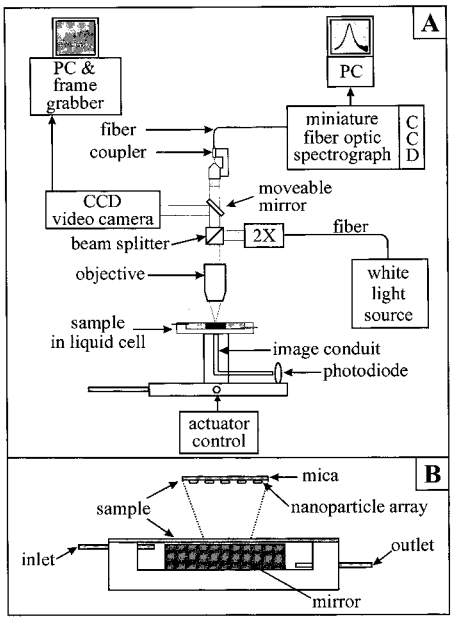

Figure 1. (A) Schematic illustration of spatially resolved UV−vis extinction spectrometer. (B) Closeup view of the liquid cell.

C. Atomic Force Microscopy (AFM) Measurements. AFM images were collected on a Digital Instruments Nanoscope III microscope under ambient conditions. Etched Si nanoprobe tips (model ESP, Digital Instruments, Santa Barbara, CA) were used. These tips have spring constants of approximately 0.15 N m^{-1} and are conical in shape with a cone angle of 20° and an effective radius of curvature at the tip of 10 nm. The AFM images presented here represent raw, unfiltered data collected in constant-force mode.

D. Ultraviolet−Visible Extinction Spectroscopy. Macroscopic UV−vis extinction measurements were performed on a Beckman DU-7 UV−vis spectrophotometer in transmission mode. Samples were placed in a thin cell cuvette, and dry nitrogen was flowed through the cell. The rectangular sample area probed by the spectrometer was approximately 2 mm × 4 mm, and the probe beam was unpolarized.

Spatially resolved UV−vis extinction measurements were performed with an Ocean Optics (Dunedin, FL) model S2000 spectrometer fiber-optically coupled to a light microscope. The instrument consists of a home-built Raman microprobe,[21] adapted such that the fiber-coupled laser input is replaced with a fiber-coupled tungsten halogen lamp (Ocean Optics, model LS-1-LL). The light exiting the 200 μm diameter core input fiber (see Figure 1A) is collimated with a GRIN lens assembly (Thorlabs, Newton, NJ), and the beam is expanded and further collimated using a home-built variable-power beam expander. The probe beam is focused through a 43× microscope objective onto the sample, which is mounted within a liquid cell (Figure 1B). The liquid cell consists of a stainless steel body with radially mounted input and output needles. A mirror is placed at the base of the cell close to the sample. The microscope objective focuses the probe beam onto the sample and collects the light that is reflected from the mirror directly under the sample. The reflected light is focused into a 400 μm diameter core optical fiber and directed into the S2000 spectrometer.

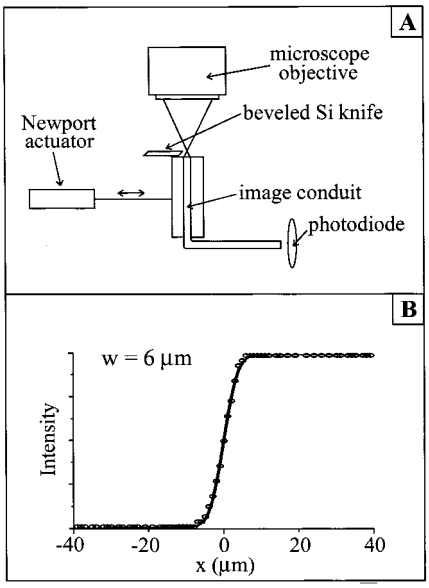

Figure 2. (A) Schematic of scanning knife edge measurement. (B) Typical intensity vs knife position data with best fit to eq 1 superimposed, corresponding to $w = 6$ μm.

III. Results and Discussion

In working with nanoparticles fabricated by nanosphere lithography, it is important to ensure that the measured extinction spectrum arises from the surface plasmon resonance of the nanoparticles themselves and not from any defect sites that are present. Defect sites are caused by packing imperfections in the polystyrene nanosphere mask, which are similar to those found in any crystal. To this end, we will first present the results of spatially resolved extinction measurements, showing that these are identical to macroscale measurements of extinction.

The first step is to determine the spatial resolution of the UV−vis microextinction spectrometer. The $1/e^2$ radius of the probe beam was measured at the focal point of the microscope objective using a scanning knife edge beam measurement technique.[22] For this measurement the liquid cell was removed and replaced by a beveled silicon knife, which was scanned across the focal point of the beam at a known velocity (Figure 2A). An image conduit (Edmund Scientific, Barrington, NJ) directed the light onto a photodiode, where the signal was measured as a function of scan time. Thus, a plot of signal intensity versus knife position could be constructed (Figure 2B). It can be shown that the transmitted light intensity measured as the knife edge cuts into a circular Gaussian beam and moves toward positive values of the x axis is

$$T(x) = \frac{1}{2}\left[1 + \mathrm{erf}\left(\frac{\sqrt{2}(x - x_o)}{w}\right)\right] \qquad (1)$$

Here, $T(x)$ is the power transmission as a function of position along the x axis. The knife position at the center of the focused beam is defined as x_o. The $1/e^2$ radius of the beam is w. Figure 2B shows the experimental data overlaid with the best-fit curve calculated using eq 1, having $w = 6$ μm.

Figure 3A shows a large-scale (62 μm × 62 μm) optical image of a typical unannealed PPA film used in this work, illustrating general film architecture and structure. There are three domains of structure in a PPA film: bare substrate, bulk silver island defects, and generally well-packed PPA areas. Representatives of each of these areas have been labeled in Figure 3A. Domains of bare substrate form as a result of multilayer packing defects present in the polystyrene nanosphere mask, which block Ag vapor from reaching the substrate. Large silver island defects result from areas of missing nanospheres in the mask, which allow Ag vapor to form large islands. The labeled PPA area consists of particles formed by a well-packed single layer of nanospheres, with some defects arising from slip dislocations and missing nanospheres in the mask. Examples of these defects can be more clearly seen in Figure 3B, which shows an AFM image (15 μm × 15 μm) taken within a well-packed PPA region. The circles drawn in parts A and B of Figure 3 represent beam-sampling areas in the spatially resolved UV−vis measurement based on a focal beam diameter of 12 μm. Figure 3C shows a more detailed view (1 μm × 1 μm) of a single hexagon of nanoparticles and the line scan of a single particle within this image. The in-plane width of the nanoparticle, measured as the perpendicular bisector of the base of the nanoparticle, is designated a, and the out-of-plane height of the nanoparticles is labeled b.

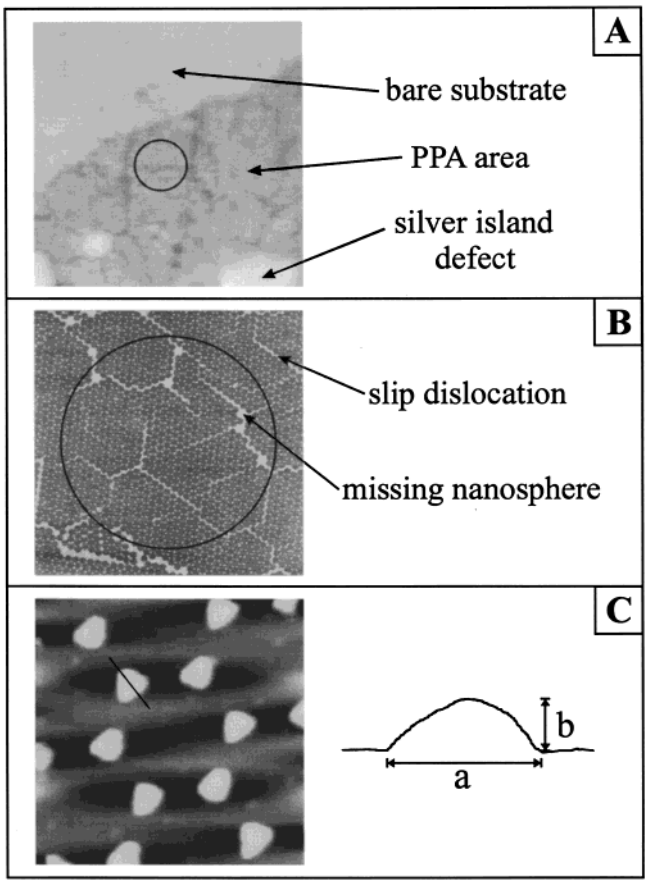

Figure 3. (A) Large-scale 62 μm × 62 μm area optical micrograph of PPA film showing domains of bare substrate, well-packed PPA region, and bulk silver island defects. Circle represents 12 μm diameter probe beam. (B) AFM image (15 μm × 15 μm) of area within well-packed PPA region. Examples of slip dislocation and missing nanosphere defects are labeled. Circle represents 12 μm diameter probe beam. (C) AFM image (1 μm × 1 μm) of a single hexagon of particles within a well-packed PPA region. Line scan across a single particle is shown, illustrating the definition of particle measurement parameters a and b.

Figure 4 presents UV−vis extinction spectra measured at 12 μm diameter resolution from eight different areas within a well-packed PPA region such as that shown in Figure 3B under ambient conditions. The wavelength corresponding to the

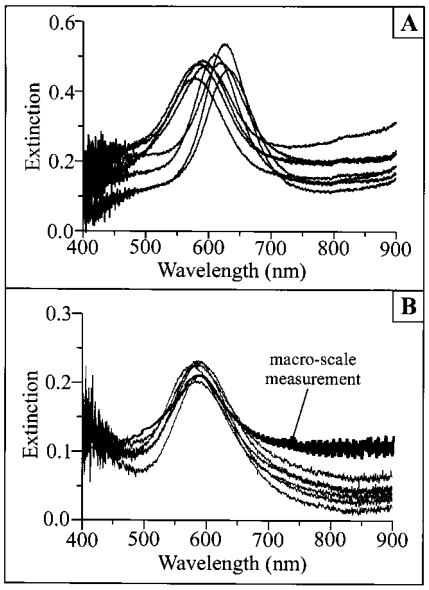

Figure 4. Spatially resolved UV−vis extinction spectra measured at 12 μm diameter resolution from eight different areas within a well-packed PPA region (A) under ambient conditions and (B) under dry N_2 conditions, with macroscale measurement overlain.

TABLE 1

sample	in-plane shape	*a* (nm), uncorrected	*a* (nm), corrected	*b* (nm)	λ_{max} (nm)
I	triangular	113 ± 8	93 ± 8	28 ± 2	650
II	triangular	120 ± 8	100 ± 8	46 ± 2	586
III	triangular	135 ± 8	115 ± 8	70 ± 2	588
IV	ellipsoidal	120 ± 8	90 ± 8	42 ± 2	426

extinction maximum of the surface plasmon resonance, λ_{max}, varies randomly from area to area between 578 and 634 nm. Figure 4B shows the variation of λ_{max} measured from the same sample after flowing dry nitrogen gas through the cell. Under these conditions, the area-to-area variation of λ_{max} was greatly diminished. We attribute the large variation in the ambient sample to local differences in dielectric environment due to a microscopically heterogeneous atmospheric water layer with random thickness.[23] The remaining differences after drying may be attributed to a combination of remnant water layer and structural heterogeneity in the particles. Since the spatially resolved spectra measured from a "dry" PPA are nearly identical to each other and to the spectrum measured macroscopically, we conclude that the presence of defect structures has a negligible effect on the surface plasmon resonance spectrum of the PPA.

We have systematically studied the effect of different solvents on the position of the surface plasmon resonance using macroscale extinction measurements for four different PPAs, labeled I−IV and described in Table 1. These PPAs were made using the same size polystyrene nanosphere deposition mask but either by varying the amount of silver deposited (samples I−III) or by annealing the particles (sample IV). Before being annealed, sample IV was structurally and optically identical to sample II. The AFM images and corresponding line scans for each PPA are shown in Figure 5. The measured lateral dimensions have not been corrected for tip-induced broadening. The "as-deposited" particles have triangular in-plane shapes regardless of height, while the annealed particles are more ellipsoidal in shape. The peak extinction wavelength, λ_{max}, for each PPA measured in a dry nitrogen environment is listed in Table 1. Note that the effect of decreasing the height of the particles is to red-shift the surface plasmon resonance frequency.

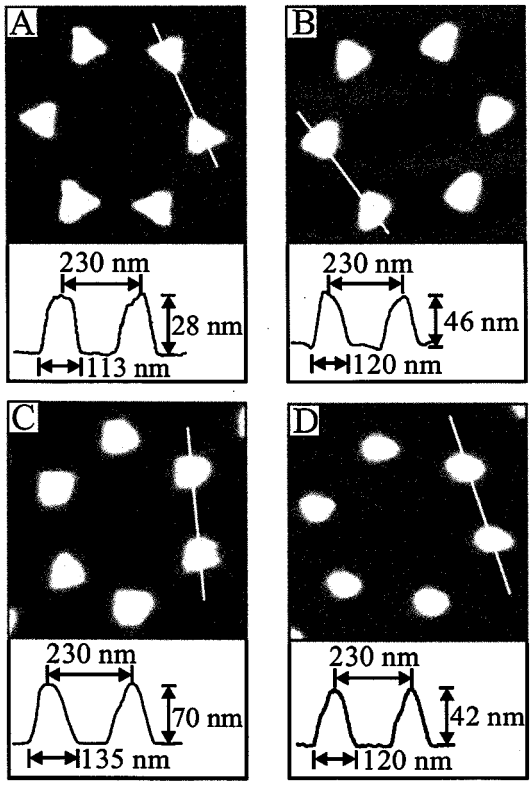

Figure 5. AFM images and line scans of Ag periodic particle arrays on mica substrates: (A) 650 nm × 650 nm image; (B) 660 nm × 660 nm image; (C) 680 nm × 680 nm image; (D) 630 nm × 630 nm image. All reported line scan values have not been deconvoluted for tip-broadening effects.

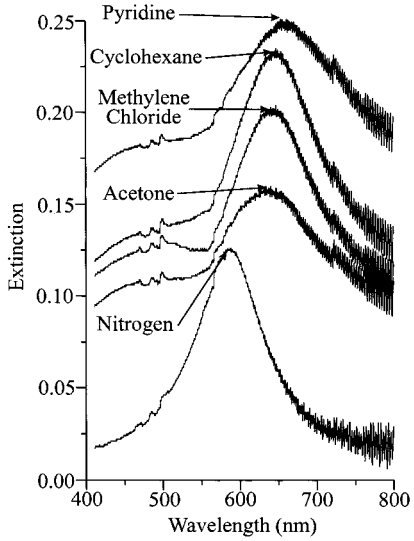

Figure 6. Extinction spectra of PPA II measured in various solvents. Spectra have been arbitrarily spaced along the extinction axis for clarity.

Also, changing the in-plane shape from triangular to circular via annealing blue-shifts the SPR by 160 nm.

Figure 6 shows the extinction spectra from PPA II immersed in various solvents. The spectra have been spaced arbitrarily along the extinction axis for better clarity. The experiment was done by drying the PPA with nitrogen and recording an initial spectrum, filling the cell with a solvent and recording the resultant spectrum, then purging the cell with nitrogen to restore the original spectrum before repeating the process with another solvent. Therefore, all the solvent shifts were completely reversible, with the exception of pyridine.

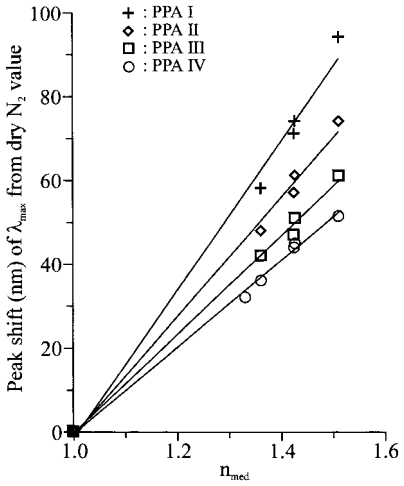

Figure 7. λ_{max}(solvent) − λ_{max}(dry nitrogen) of the localized surface plasmon resonance vs the refractive index of the solvent for each PPA sample.

Figure 7 plots the value of λ_{max}(solvent) − λ_{max}(dry nitrogen) of the surface plasmon resonance for each PPA as a function of the refractive index of the surrounding medium, n_{med}. We have plotted the data as a function of peak wavelength shift from the dry nitrogen value in order to normalize the data and better compare the slopes for each PPA. Within this range of n_{med}, the data points for each PPA can be fitted reasonably well to a straight line. We find that the PPA having the shortest height (b = 28 nm, sample I) is most sensitive to changes in the surrounding dielectric medium followed by PPA II (b = 46 nm), then PPA III (b = 70 nm), and lastly the annealed PPA IV (b = 42 nm). For the most sensitive PPA (sample I), we can calculate on the basis of the slope of the line of peak shift vs n_{med} that every 0.005 change in the refractive index of the solvent will produce a change in the extinction peak maximum of approximately 1 nm.

IV. Theory: Discrete Dipole Approximation (DDA)

The DDA is a numerical approximation of Maxwell's equations, which can calculate the absorption, scattering, and extinction cross sections nearly exactly for particles of arbitrary shape. It involves replacing the particle of interest by a cubic array of dipoles, each of which has an oscillating polarization that is determined by the local dielectric constant, the incoming electromagnetic field, and interaction with other dipoles. The optical response of the collection of dipoles to the applied field can then be described by self-consistently determining the induced dipole in each element. The full details of the method have been previously discussed.[24−26] We have used an adaptation of a program[27] developed by Draine and Flatau that utilizes fast Fourier transform methods to sum over the dipole fields.

To use the DDA to model the optical properties of nanoparticles produced via nanosphere lithography, we must know the size, shape, and dielectric properties of the nanoparticle. The size of the nanoparticles is known from AFM measurements. We will approximate the shape of the annealed particles as oblate ellipsoids and that of the "as-deposited" particles as truncated tetrahedra on the basis of their AFM line scan shapes.[19] The measured lateral dimensions of the nanoparticle must be corrected for tip-broadening effects. This is done by tracking the motion of a conical AFM tip with a radius of curvature of 10 nm and a 20° cone angle over an ideal oblate ellipsoid or truncated tetrahedron with the measured height b and subtracting the amount of tip convolution from the measured in-plane widths a.[17] The results of applying this procedure to correct the measured in-plane widths are shown in Table 1. The wavelength-dependent bulk dielectric constants for silver from Palik[28] have been used in all calculations. Unless otherwise stated, we model only single isolated nanoparticles, neglecting the effects of particle−particle and particle−substrate interactions. The effect of substrate is directly modeled in some calculations by including a cylindrical substrate slab as part of the target geometry. This is a different method of including substrate interactions compared with the method in our previous work,[19] and we find that it leads to better and more understandable results.

According to Mie theory, the cross section of extinction of a homogeneous spherical particle in an isotropic medium is

$$C_{ext} = \frac{2\pi}{k^2}\sum_{\upsilon=1}^{\infty}(2\upsilon + 1)\,\mathrm{Re}(a_\upsilon + b_\upsilon) \tag{2}$$

where $k = 2\pi n_{med}/\lambda$ and a_υ and b_υ are the so-called Mie coefficients expressed in terms of Ricatti−Bessel functions. The refractive index of the external medium, n_{med}, is related to the dielectric constant by $\epsilon_{med} = n_{med}^2$. To a first approximation, only the first term in the series ($\upsilon = 1$) is important and $a_\upsilon \gg b_\upsilon$. Solving eq 2, we find that the extinction cross section is proportional to an expression involving the dielectric function of both the sphere material (ϵ) and the medium (ϵ_{med}):

$$C_{ext} = \frac{4\pi}{k^2}\,\mathrm{Re}\left(\mathrm{i}\left(\frac{\epsilon - \epsilon_{med}}{\epsilon + 2\epsilon_{med}}\right)\right) \tag{3}$$

Therefore, the resonance condition occurs when

$$\mathrm{Re}(\epsilon + 2\epsilon_{med}) \rightarrow 0 \tag{4}$$

Assuming the sphere material is an ideal free-electron metal, we can write an expression for ϵ using the Drude model,

$$\mathrm{Re}(\epsilon) = 1 - \frac{\omega_p^{\,2}}{\omega^2 + \gamma^2} \tag{5}$$

where ω_p is the plasmon frequency of the bulk metal and γ is the damping frequency of the bulk metal. In the visible and ultraviolet regions of the spectrum, $\gamma \ll \omega_p$, and therefore, the Drude equation can be simplified to good approximation:

$$\mathrm{Re}(\epsilon) = 1 - \frac{\omega_p^{\,2}}{\omega^2} \tag{6}$$

At resonance then,

$$\omega = \frac{\omega_p}{\sqrt{2\epsilon_{med} + 1}} \tag{7}$$

or

$$\lambda = \lambda_p\sqrt{2\epsilon_{med} + 1} \cong \sqrt{2}\lambda_p n_{med} \tag{8}$$

Therefore, within a sufficiently narrow range of n_{med}, a plot of peak resonance wavelength versus the refractive index of the surrounding medium should be linear.

We have incorporated an external dielectric medium into the DDA program by making two approximations. The first of these is that the effective dielectric function of the metal particle

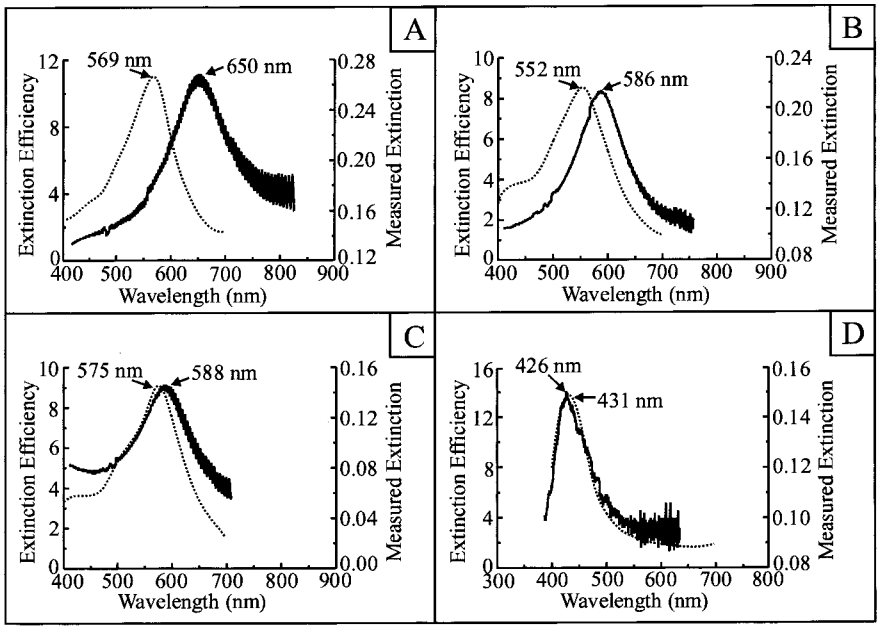

Figure 8. DDA theory results (dashed lines) compared to experimental measurements for each PPA sample using tip-corrected AFM measurements: (A) PPA I, truncated-tetrahedron geometry with 22 081 dipoles; (B) PPA II, truncated-tetrahedron geometry with 10 548 dipoles; (C) PPA III, truncated-tetrahedron geometry with 27 522 dipoles; (D) PPA IV, oblate ellipsoid geometry with 22 329 dipoles.

surrounded by a medium of dielectric constant ϵ_{med} can be described as

$$\epsilon_{metal,eff} = \frac{\epsilon_{metal}}{\epsilon_{med}} \tag{9}$$

Second, we use an effective wavelength λ_{eff}, where

$$\lambda_{eff} = \frac{\lambda_{vac}}{n_{med}} \tag{10}$$

Incorporating these approximations, we can calculate the extinction of a truncated tetrahedron or oblate ellipsoid immersed in a solvent.

Figure 8 shows the calculated extinction spectrum for each PPA compared to the measured extinction spectrum in a dry nitrogen environment. The DDA calculations are based on the tip-corrected AFM measurements, using the truncated-tetrahedron geometry for the "as-deposited" PPAs (samples I−III) and an oblate ellipsoid geometry for the annealed PPA (sample IV). The assumption of an oblate spheroid geometry for PPA IV is somewhat arbitrary but provides at least a reasonable approximation to the shape produced in the annealing process. No adjustable parameters have been used in the calculation. Details of the match between theory and experiment for PPA sample II have been thoroughly discussed in a previous paper.[19] The discrepancy between the theoretical and experimental results is very small for the oblate ellipsoid PPA (sample IV). However, the discrepancy becomes progressively greater for the truncated-tetrahedron-shaped PPAs as their out-of-plane height decreases and they become more oblate.

We have included a cylindrical slab of mica directly touching the silver particle in the calculations presented in Figure 9. Since the short truncated-tetrahedron-shaped particle has more direct contact with the substrate, it is further red-shifted by the inclusion of substrate interactions than the oblate ellipsoid-shaped particle. Therefore, we find that including the effect of substrate in the calculations provides a better match to experimental results. The match for PPA IV is not quite as good as

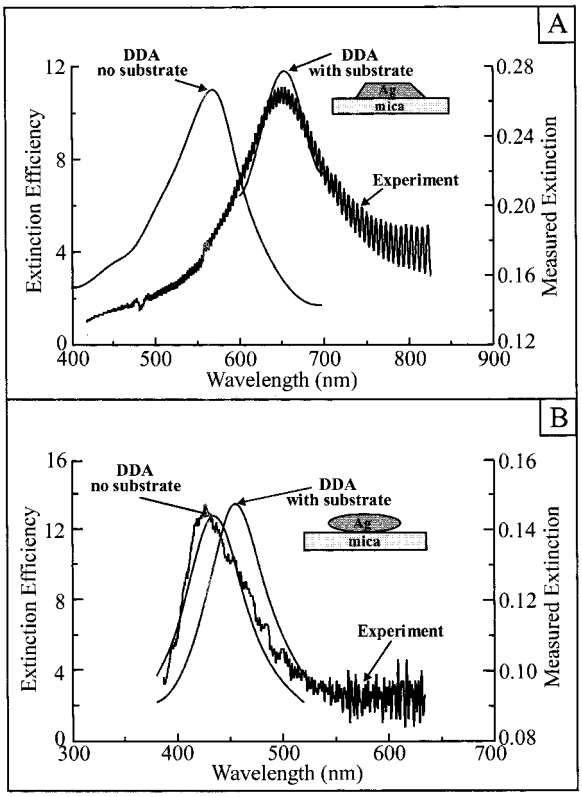

Figure 9. DDA theory results calculated using cylindrical mica slab in target geometry compared to experimental measurements. Also included for reference are the calculations from Figure 8 using no substrate. (A) For PPA I, the silver truncated tetrahedron has 9982 dipoles and the cylindrical mica slab is 30 nm thick and 153 nm in diameter and contains 63 126 dipoles. (B) For PPA IV,the silver oblate ellipsoid has 6632 dipoles and the cylindrical mica slab is 45 nm thick and 120 nm in diameter and contains 18 855 dipoles.

for PPA I, but since our knowledge of the structure of PPA IV is less certain than PPA I, the observed agreement is still reasonable. This is an expensive calculation, since a large number of dipoles must be used to ensure convergence of the

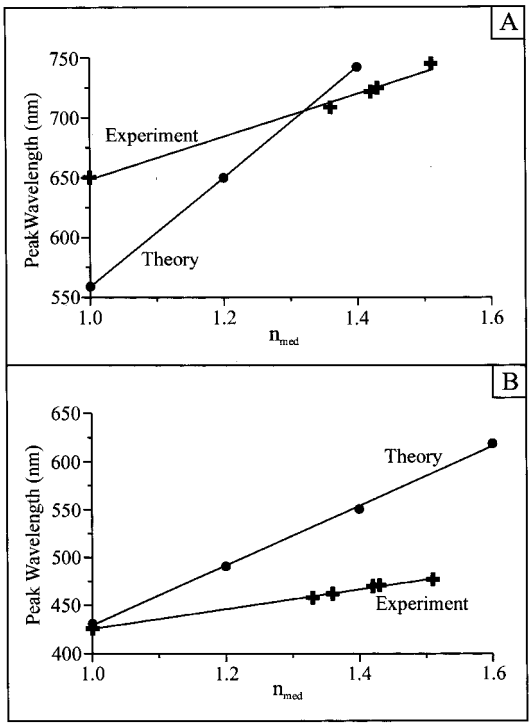

Figure 10. λ_{max} of the localized surface plasmon resonance vs the refractive index of the solvent, showing experiment vs theory: (A) PPA I, $a = 93$ nm, $b = 28$ nm; (B) PPA IV, $a = 90$ nm, $b = 42$ nm, annealed.

combined mica and silver target. We find that in order to obtain a reasonably converged result, the thickness of the mica slab must be approximately the same thickness as the silver particle. The slab of mica must extend past the edge of the silver particle by approximately a particle radius. The dipole grid spacing is constant and the same in both the silver particle and the touching mica slab.

The calculated effect of solvent on the extinction spectrum of PPA samples I and IV is shown in Figure 10. For both the "as-deposited" sample I and the annealed sample IV, the DDA calculation predicts a larger extinction red shift due to the presence of solvent than is observed experimentally. The effect of the external dielectric medium was calculated both with and without the presence of a mica substrate slab (Figure 10 shows the result without), and in both cases the calculated result was more red-shifted than the experimental result. We have also modeled the effect of solvent directly by including a several-dipoles-thick solvent shell around the silver particle and mica slab target, reaching the same result.

V. Conclusions

The results presented in this paper show that the extinction spectra of nanofabricated silver particles are much more sensitive to the dielectric properties of the surrounding medium than has been previously appreciated. As the refractive index of the surrounding medium increases, the extinction maximum of the nanoparticles red-shifts in wavelength. There is an approximately linear relationship between the λ_{max} of extinction and the refractive index of the external dielectric medium for the values of refractive index that we examined. The extinction spectrum of nanoparticles that were oblate ellipsoidal in shape was least sensitive to the refractive index of the external medium, while the truncated-tetrahedron-shaped nanoparticles with the smallest out-of-plane height were the most sensitive. We find that the most sensitive nanoparticles can sense a 0.005 change in the refractive index of the external medium, resulting in a 1 nm shift in the extinction maximum of the surface plasmon resonance.

The spatially resolved UV−vis extinction measurements at 12 μm resolution are nearly equivalent to the macroscale measurements when the sample is in a dry nitrogen environment. Thus, defect sites present in the nanoparticle array play a negligible role in the extinction measurements.

The DDA theory can be used to quantitatively model the extinction spectra of both the as-deposited and annealed nanoparticles. There are no adjustable parameters used in the calculation. The size of the nanoparticles is obtained directly from tip-corrected AFM measurements, and the shape of the nanoparticle is estimated on the basis of AFM images and line scans. In a dry nitrogen environment, the match between the DDA-calculated results and the experimentally measured results is best for the ellipsoidal-shaped particles. As the particle shape becomes more oblate, the discrepancy between theory and experiment increases. This is shown to be due in part to particle−substrate interactions. The shortest truncated tetrahedron (PPA I) has the most contact with the mica substrate, and therefore, its extinction spectrum is most red-shifted by including the effect of substrate. The oblate ellipsoid (PPA IV) has the least contact with the substrate, and its extinction spectrum is affected less by the inclusion of substrate effects.

The DDA theory predicts a larger red-shifting in the extinction maximum with increasing solvent refractive index than is seen experimentally. However, the theory qualitatively describes the effect of external solvent on the surface plasmon resonance, which to the best of our knowledge has not been previously done for nonspherical particles. At this time we are unsure of the cause of the discrepancy between theory and experiment; however, the fact that the theory overestimates the solvent shift suggests that the solvent is not in immediate contact with the metal surface. One reason this might occur, which has been considered in ellipsometry measurements on silver and copper films,[29] is the formation of an oxide layer on the particle surfaces. To study this effect, we would like to calculate the effect of an oxide layer surrounding our silver nanoparticles on the surface plasmon resonance. This calculation, however, is computationally prohibitive with our current resources. We have also begun to address these questions experimentally by chemically modifying the nanoparticles using self-assembled monolayers. This should provide a better understanding of the effect of adsorbed species on the surface plasmon resonance spectra.

Acknowledgment. This research was supported by ARO Grant DAAG55-97-1-0133, National Science Foundation Grant CHE-940078, and MRSEC program of the National Science Foundation Grant DMR-9632472.

References and Notes

(1) Bohren, C. F.; Huffman, D. R. *Absorption and Scattering of Light by Small Particles*; John Wiley & Sons: New York, 1983.

(2) Schatz, G. C. *Acc. Chem. Res.* **1984**, *17*, 370−376.

(3) Mulvaney, P. *Langmuir* **1996**, *12*, 788−800.

(4) Taleb, A.; Petit, C.; Pileni, M. P. *J. Phys. Chem. B* **1998**, *102*, 2214−2220.

(5) Creighton, J. A.; Eadon, D. G. *J. Chem. Soc., Faraday Trans.* **1991**, *87*, 3881−3891.

(6) Alvarez, M. M.; Khoury, J. T.; Schaaff, T. G.; Shafigullin, M. N.; Vezmar, I.; Whetten, R. L. *J. Phys. Chem. B* **1997**, *101*, 3706−3712.

(7) Kreibig, U.; Vollmer, M. *Optical Properties of Metal Clusters*; Springer-Verlag: Heidelberg, Germany, 1995; Vol. 25.

(8) Papavassiliou, G. C. *Prog. Solid State Chem.* **1980**, *12*, 185−271.

(9) Lee, M. H.; Dobson, P. J.; Cantor, B. *Thin Solid Films* **1992**, *219*, 199−205.

(10) Shklyarevskii, I. N.; Anachkova, E.; Blyashenko, G. S. *Opt. Spectrosc.* **1977**, *43*, 427−429.

(11) Van Duyne, R. P.; Hulteen, J. C.; Treichel, D. A. *J. Chem. Phys.* **1993**, *99*, 2101−2115.

(12) Hornyak, G. L.; Patrissi, C. J.; Martin, C. R. *J. Phys. Chem. B* **1997**, *101*, 1548−1555.

(13) Hornyak, G. L.; Martin, C. R. *Thin Solid Films* **1997**, *303*, 84−88.

(14) Gotschy, W.; Vonmetz, K.; Leitner, A.; Aussenegg, F. R. *Opt. Lett.* **1996**, *21*, 1099−1101.

(15) Gotschy, W.; Vonmetz, K.; Leitner, A.; Aussenegg, F. R. *Appl. Phys. B* **1996**, *63*, 381−384.

(16) Buncick, M. C.; Warmack, R. J.; Ferrell, T. L. *J. Opt. Soc. Am. B* **1987**, *4*, 927−933.

(17) Hulteen, J. C.; Treichel, D. A.; Smith, M. T.; Duval, M. L.; Jensen, T. R.; Van Duyne, R. P. *J. Phys. Chem. B* **1999**, 3854−3863.

(18) Hulteen, J. C.; Van Duyne, R. P. *J. Vac. Sci. Technol. A* **1995**, *13*, 1553−1558.

(19) Jensen, T. R.; Schatz, G. C.; Van Duyne, R. P. *J. Phys. Chem. B* **1999**, *103*, 2394−2401.

(20) Hulteen, J. C.; Smith, M. T.; Van Duyne, R. P. *J. Phys. Chem. B*, in preparation.

(21) Van Duyne, R. P.; Haller, K. L.; Altkorn, R. I. *Chem. Phys. Lett.* **1986**, *126*, 190−196.

(22) Suzaki, Y.; Tachibana, A. *Appl. Opt.* **1975**, *14*, 2809−2810.

(23) Piner, R. D.; Mirkin, C. A. *Langmuir* **1997**, *13*, 6864−6868.

(24) Draine, B. T.; Flatau, P. J. *J. Opt. Soc. Am. A* **1994**, *11*, 1491.

(25) Yang, W. H.; Schatz, G. C.; Van Duyne, R. P. *J. Chem. Phys.* **1995**, *103*, 869−875.

(26) Jensen, T.; Kelly, L.; Lazarides, A.; Schatz, G. C. *J. Cluster Sci.* **1999**, *10*, 295−317.

(27) Draine, B. T.; Flatau, P. J. *Program DDSCAT*; University of California, San Diego, Scripps Institute of Oceanography: La Jolla, CA.

(28) Palik, E. D. *Handbook of Optical Constants of Solids*; Academic Press: New York, 1985.

(29) Wissmann, P. Optical Properties of Thin Metal Films Interacting with Gases. In *Handbook of Optical Properties. Optics of Small Particles, Interfaces, and Surfaces*; Hummel, R. E., Wissmann, P., Eds.; CRC Press: Boca Raton, FL, 1997; Vol. II, pp 401−446.